Theoretical approach and experimental investigation of spin current tunnelling in $Ni_{80}Fe_{20}/Si_3N_4/Fe_{40}Co_{37}Zr_{11}N_{12}$ magnetically collinear trilayer films with defined in-plane uniaxial anisotropy

K. Seemann

Karlsruhe Institute of Technology KIT (Campus North), Institute for Applied Materials, Hermann–von–Helmholtz–Platz 1, 76344 Eggenstein-Leopoldshafen, Germany

A B S T R A C T

Ferromagnetic trilayer film systems with nonferromagnetic Si_3N_4 interface layers were fabricated by using magnetron sputtering. A post-annealing process was carried out at 400 °C for 2 h in a static magnetic field, in order to induce an in-plane uniaxial anisotropy. The present study introduces the exchange interaction between ferromagnetic layers which influences the static magnetisation properties as well as the natural resonance frequency behaviour and its damping features, i.e., damping and anti-damping effects. This is expressed by the total damping parameter $\alpha_i^{tot} = \alpha_{Gi} \pm \alpha_{spi}$, which is enhanced or reduced by a spin transfer torque damping parameter $\pm \alpha_{spi}$ whereupon Gilbert bulk damping α_{Gi} is considered to be independent. The static polarisation loops are slightly but noticeably different, caused by an interface with thickness up to 100 nm, which reflects a decreasing exchange interaction. With varying the interface thickness, the films also show a distinct variation in their frequency spectra. This leads to the conclusion that spin currents caused by spin pumping arise, and tunnelling within a Si_3N_4 insulating barrier generates spin transfer torque. This can be assumed because the observed ferromagnetic resonance dual lines show remarkable changes in their Full Width at Half Maxima (FWHM) at frequencies of approximately 600 MHz caused by the $Ni_{80}Fe_{20}$ layers and 2.32 GHz caused by the $Fe_{40}Co_{37}Zr_{11}N_{12}$ layers. Regarding the FWHM of the resonance frequency spectra in association with the damping constant α_{eff} on the dependence of the interface layer thickness, one can observe an exponential curve shape for both ferromagnetic layers, which is obviously a sign for the interaction between the layers through a spin current tunnelling mechanism.

1. Introduction

The world of magnetic film materials for spintronics has been facing ongoing challenges due to the demand of higher performance of MRAMS, spin valves for read heads. Even magnetic sensor applications, which monitor mechanical load [1–3], could benefit from these film materials. This research area obviously turns out to be inexhaustible due to the fact, that many applications have not been reconsidered yet for which spintronic effects might be useful. For sure, most applications have one thing in common. They depend on their magnetic spin dynamic damping features, which also influence their resonance behaviour if exposed to a high-frequency electromagnetic wave. Especially, in thin ferromagnetic single films the shape of resonance spectra is extensively investigated in terms of precession damping. Precession damping of the magnetic moments are not only associated with the intrinsic damping by Zeeman transition and 3d itinerant electron spin interaction with cations

(spin–orbit coupling) or extrinsic damping by two-magnon scattering with nonmagnetic impurities, voids or dislocations. There are additional damping properties, which influence spin dynamics if, e.g., two magnetic films (F1, F2) are combined with an insulating nonmagnetic interface layer (N) between. At this point, spin current tunnelling between the two ferromagnetic film layers (F1/N/F2) excited by ferromagnetic resonance (FMR), which generates spin transfer torque, plays a decisive role. This leads to spontaneous precession or switching of magnetic moments as well as the increase or decrease of damping in the on-resonance layers, respectively. In literature, the theory and experiments of spin transfer torque can help to understand the spin current flow by high-frequency spin excitation in a normal metal interface layer towards or between magnetic layers [4–8], but for insulating interface layers few works has been done on high-frequency spin pumping by now only [9–13].

In the present paper, we like to focus our basic research on two

different ferromagnetic film materials separated by a Si_3N_4 interface layer, which is frequently used in the semiconductor/microelectronic technology as a classical insulating and/or passivating layer. As an insulator it implies spin tunnelling between the ferromagnetic layers during the spin pumping process.

Despite spin pumping across insulators decreases quickly, there is a dynamic interaction between the ferromagnetic layers caused by tunnelling of spin currents through the insulator. As tunnelling is assumed a strong exponential decay of the spin current is probable [9]. Consequently, transmission and reflection is common if magnetic electron spins face a barrier of certain thickness. During the tunnelling process the magnetic spins lose angular momentum by scattering or/and meet backflow to the on-resonance layer. So, one has to settle the question how damping by spin transfer torque in those trilayer systems acts on the resonance precession of each ferromagnetic layer. Beside experimental work we try to present a theoretical, even though, a qualitative approach of electron spins which face a barrier of certain height they may tunnel through, in order to interact with the macro spin of two different ferromagnetic layers, respectively. In order to gain, for the first time, a rudimentary but detailed understanding of the process, a theoretical model shall be established. With the upcoming experiments a direct comparison between the model and measurement ought to give a background and inducement for further research on those film combinations. The impressive ansatz of [14,15] considering metallic interfaces provide a useful introduction. It helps to create an advanced exemplary model of tunnelling between ferromagnetic layers.

2. Theoretical considerations of a trilayer spin current tunnel system

2.1. Quantum mechanical approach

The model bases on a following assumption that a spin current formed by spin up↑ and down ↓ electrons is emitted by two ferromag-

For convenience, one can make the ansatz for a one-dimensional plane wave function which represents the superposition of two electron spin up (+) and down (-) wave functions as follows.

$$\psi(x) \quad \psi_+(x) + \psi_-(x)$$

Assuming, that there is a rotation of spins by θ or φ with respect to the z-direction (normal to the propagation in x-direction) one has to apply the rotation operator for which, after the normalisation process and after going through the steps of matching conditions, the resulting spinor wave functions have the following form:

$$\psi_{in}^{\pm}(x) \quad \sqrt{\frac{T_+}{2a}} \bullet e^{ik_+ x} \bullet cos\frac{\theta}{2}|+\rangle + \sqrt{\frac{T_-}{2a}} \bullet e^{ik_- x} \bullet sin\frac{\theta}{2} \bullet e^{-i\varphi}|-\rangle \quad (2)$$

$$\psi_{refl}^{\pm}(x) \quad \sqrt{\frac{T_+ \bullet (1 - \widetilde{T}_+)}{2a}} \bullet e^{-ik_+ x} \bullet cos\frac{\theta}{2}|+\rangle + \sqrt{\frac{T_- \bullet (1 - \widetilde{T}_-)}{2a}} \bullet e^{-ik_- x}$$
$$\bullet sin\frac{\theta}{2} \bullet e^{-i\varphi}|-\rangle \quad (3)$$

$$\psi_{trans}^{\pm}(x) \quad \sqrt{\frac{T_+ \bullet \widetilde{T}_+}{2a}} \bullet e^{i\widetilde{k}_+ x} \bullet cos\frac{\theta}{2}|+\rangle + \sqrt{\frac{T_- \bullet \widetilde{T}_-}{2a}} \bullet e^{i\widetilde{k}_- x} \bullet sin\frac{\theta}{2} \bullet e^{-i\varphi}|-\rangle$$

They represent the incoming (2), reflected (3) as well as transmitted wave (4) for $\times \geq 0$. |+> and |-> are spin states for the spin up and spin down electrons with wave numbers $k_{+/-}$ and $\widetilde{k}_{+/-}$.

The transmission coefficients for a tunnel barrier with height $U_b(t_{int}) > E_+$ and thickness t_{int} would be.

$$T_+ \quad \frac{4 \bullet E_+ \bullet (U_b(t_{int}) - E_+)}{4 \bullet E_+ \bullet (U_b(t_{int}) - E_+) + U_b^2(t_{int}) \bullet sinh^2\left(\sqrt{2 \bullet m_e \bullet (U_b(t_{int}) - E_+)} \bullet \frac{t_{int}}{\hbar}\right)} \quad (5)$$

for the spin up electrons (minority electrons) and.

$$T \quad \frac{4 \bullet (E_+ + \Delta E_{ex}) \bullet (U_b(t_{int}) - (E_+ + \Delta E_{ex}))}{4 \bullet E_+ \bullet (U_b(t_{int}) - (E_+ + \Delta E_{ex})) + U_b^2(t_{int}) \bullet sinh^2\left(\sqrt{2 \bullet m_e \bullet (U_b(t_{int}) - (E_+ + \Delta E_{ex}))} \bullet \frac{t_{int}}{\hbar}\right)} \quad (6)$$

netic layers, alternately being on resonance and face an insulating interface layer (F1/N/F2) acting as a tunnel barrier of certain height U_b and width t_{int}. Dependent on whether reflection or transmission occurs, the electron with spin ½ up or ½ down then strikes a potential step U_{p1} at the boundary of the opposite ferromagnetic layer, or vice versa (U_{p2}). In general, one can regard a spin current which can pass two potentials or is (partially) reflected, as illustrated in Fig. 1.

The illustrative model shows two different ferromagnetic films with different Fermi energies E_{F1} and E_{F2}. The exemplary approach of the tunnel system uses an insulating interface layer, which possesses a Fermi energy E_F^{int} lower than the Fermi energies of the magnetic material. Dependent on the energy gap E_g of the interface layer the potential barrier $U_b(x)$ $E_F^{int} + E_g/2$, is considered as a work function and is about constant over t_{int}. Due to this arrangement the Fermi energies are now smeared at the boundaries, so that E_{F1} and E_{F2} are now effective Fermi energies at $\times$ 0, respectively. They are just below $U_b(x)$.

for the spin down electrons (majority electrons). These formulas are known but are simply modified. The energy of the spin down electrons shifts to a higher energy state due to the exchange field splitting by ΔE_{ex}

$g \cdot \mu_B \mu_0 H_{ex}$ where g is the splitting factor, μ_B the Bohr magneton and $\mu_0 H_{ex}$ the exchange field of the respective ferromagnetic layer. The energy E_+ can be assumed to be in the range of the Fermi energy of the ferromagnetic layer that is just on resonance. The parameter m_e is the effective electron mass. On the other side, when the tunnel barrier potential is $U_b(t_{int}) < E_+$, the transmission coefficients possess the following form.

$$T_+ \quad \frac{4 \bullet E_+ \bullet (E_+ - U_b(t_{int}))}{4 \bullet E_+ \bullet (E_+ - U_b(t_{int})) + U_b^2(t_{int}) \bullet sin^2\left(\sqrt{2 \bullet m_e \bullet (E_+ - U_b(t_{int}))} \bullet \frac{t_{int}}{\hbar}\right)} \quad (7)$$
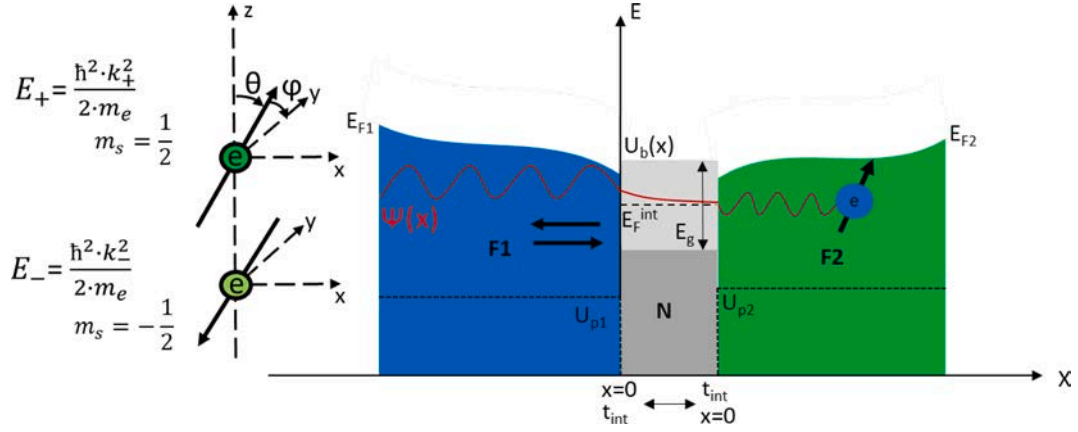
$$T \quad \frac{4 \bullet (E_+ + \Delta E_{ex}) \bullet ((E_+ + \Delta E_{ex}) - U_b(t_{int}))}{4 \bullet E_+ \bullet ((E_+ + \Delta E_{ex}) - U_b(t_{int})) + U_b^2(t_{int}) \bullet sin^2\left(\sqrt{2 \bullet m_e \bullet ((E_+ + \Delta E_{ex}) - U_b(t_{int}))} \bullet \frac{t_{int}}{\hbar}\right)} \quad (8)$$

Fig. 1. Schematic of the tunnel process for a spin current between two different ferromagnetic films separated by an insulating interface layer, which forms a tunnel barrier $U_b(x) \approx$ const., as well as potential steps U_p in the ferromagnetic layers.

and may show resonant tunnelling.

After the electron spin current has passed the tunnel barrier they face a potential step U_p. This quantity is set equal the splitting energy of the respective magnetic layer and is lower than the electron energy ($U_p < E_+$). At this point, the transmission coefficients result in.

$$\widetilde{T}_+ \quad \frac{4 \bullet \sqrt{E_+ \bullet (E_+ \quad U_p)}}{2 \bullet E_+ \quad U_p + 2 \bullet \sqrt{E_+ \bullet (E_+ \quad U_p)}} \tag{9}$$

and.

$$\widetilde{T} \quad \frac{4 \bullet \sqrt{(E_+ + \Delta E_{ex}) \bullet (E_+ + \Delta E_{ex} \quad U_p)}}{2 \bullet (E_+ + \Delta E_{ex}) \quad U_p + 2 \bullet \sqrt{(E_+ + \Delta E_{ex} \quad U_p) \bullet (E_+ + \Delta E_{ex})}}$$

In accordance with the transmission coefficients the general reflection coefficients are R 1-T. The effective energy of the spin carrying electron of the i-th ferromagnetic layer is defined by.

$$E_{i+} \quad E_{Fi} + \frac{3}{2} \bullet k_B \bullet T + \hbar \bullet \omega_{iFMR} \quad i \quad 1, 2 \tag{11},$$

where k_B is the Boltzmann constant, T is the temperature, $\hbar$ is the Plancks constant and ω_{iFMR} $2\pi f_{FMR}$ (Ferro Magnetic Resonance).

In order to determine the spin current, their transverse and longitudinal contributions, i.e., the incident spin directions perpendicular and parallel to the magnetisation are expressed as follows.

The transverse spin current can now be described by the equations.

$$\mathscr{S}_{xx}^{in} \quad \frac{\hbar^2 \bullet k_+}{4 \bullet m_e \bullet a} \bullet \left(\sqrt{T_+ \bullet T} \quad \bullet \sin\theta \bullet \cos\varphi \right) \tag{12}$$

$$\mathscr{S}_{xx}^{trans} \quad \frac{\hbar^2 \bullet k_+}{4 \bullet m_e \bullet a} \bullet \left(\sqrt{T_+ \bullet T} \quad \bullet \widetilde{T}_+ \bullet \widetilde{T} \quad \bullet \sin\theta \bullet \cos\varphi \right) \tag{13}$$

$$\mathscr{S}_{xx}^{ref} \quad \frac{\hbar^2 \bullet k_+}{4 \bullet m_e \bullet a} \bullet \left(\sqrt{T_+ \bullet T} \quad \bullet \widetilde{R}_+ \bullet \widetilde{R} \quad \bullet \sin\theta \bullet \cos\varphi \right) \tag{14}$$

$$\mathscr{S}_{xy}^{in} \quad \frac{\hbar^2 \bullet k_+}{4 \bullet m_e \bullet a} \bullet \left(\sqrt{T_+ \bullet T} \quad \bullet \sin\theta \bullet \sin\varphi \right) \tag{15}$$

$$\mathscr{S}_{xy}^{trans} \quad \frac{\hbar^2 \bullet k_+}{4 \bullet m_e \bullet a} \bullet \left(\sqrt{T_+ \bullet T} \quad \bullet \widetilde{T}_+ \bullet \widetilde{T} \quad \bullet \sin\theta \bullet \sin\varphi \right) \tag{16}$$

$$\mathscr{S}_{xy}^{ref} \quad \frac{\hbar^2 \bullet k_+}{4 \bullet m_e \bullet a} \bullet \left(\sqrt{T_+ \bullet T} \quad \bullet \widetilde{R}_+ \bullet \widetilde{R} \quad \bullet \sin\theta \bullet \sin\varphi \right)$$

The longitudinal contributions are.

$$\mathscr{S}_{xz}^{in} \quad \frac{\hbar^2 \bullet k_+}{4 \bullet m_e \bullet a} \bullet \left(T_+ \bullet \cos^2\frac{\theta}{2} \quad T \quad \bullet \sin^2\frac{\theta}{2} \right) \tag{18}$$

$$\mathscr{S}_{xz}^{trans} \quad \frac{\hbar^2 \bullet k_+}{4 \bullet m_e \bullet a} \bullet \left(T_+ \bullet \widetilde{T}_+ \bullet \cos^2\frac{\theta}{2} \quad T \quad \bullet \widetilde{T} \quad \bullet \sin^2\frac{\theta}{2} \right) \tag{19}$$

$$\mathscr{S}_{xz}^{ref} \quad \frac{\hbar^2 \bullet k_+}{4 \bullet m_e \bullet a} \bullet \left(T_+ \bullet \widetilde{R}_+ \bullet \cos^2\frac{\theta}{2} \quad T \quad \bullet \widetilde{R} \quad \bullet \sin^2\frac{\theta}{2} \right)$$

Generally, the $\mathbf{S}^{in}$ represent the spin currents transmitted by the tunnel barrier. The $\mathbf{S}^{trans}$ and $\mathbf{S}^{ref}$ are the spin currents, which are transmitted or reflected at the insulator/ferromagnet interface on the dependence of the tunnel barrier thickness, i.e., the interface layer thickness. Whilst the longitudinal current (θ φ 0) does not contribute to torque the transverse spin currents (θ $\pi/2$ and φ 0 or θ $\pi/2$ and φ $\pi/2$) do, which increase or lower precession damping of the spin system in the individual ferromagnetic layer.

The resulting spin current is then defined by.

$$\mathscr{S}_{sc} \quad \left(\mathscr{S}_{xx}^{in} + \mathscr{S}_{xy}^{in} + \mathscr{S}_{xx}^{ref} + \mathscr{S}_{xy}^{ref} \right) \quad \left(\mathscr{S}_{xx}^{trans} + \mathscr{S}_{xy}^{trans} \right)$$

In Fig. 2, the curves represent a general and qualitative computation of the spin current densities, which propagate, for instance, from

Fig. 2. Resulting spin current density dependent on the interface layer thickness t_m. The tunnelling model generates different curve shapes, which follow from the variation (gradual decrease) of the tunnel barrier height expressed by means of E_g (E_g 1 > E_g 4).

$Fe_{40}Co_{37}Zr_{11}N_{12}$ to $Ni_{80}Fe_{20}$. It can be observed that the spin current exponentially drops within an interlayer thickness of a few nanometres. By varying the tunnel barrier height expressed through the energy gap E_g, the curves show clear maxima, which arises due to the assumption that the electron spin energy can be close to the barrier potential, i.e., close to resonant tunnelling.

If the tunnel barrier is high enough ordinary tunnelling would dominate.

2.2. Frequency dynamics of the trilayer film configuration

If the ferromagnetic films/insulating interface layer arrangement is exposed to a transversal in-plane high frequency field the magnetic moments, which can be considered as a macro spin, precess about the direction of an effective magnetic field H_{effi} dominated by the in-plane uniaxial anisotropy H_{ui} and the saturation magnetisation M_{si}. The Landau-Lifschitz-Gilbert differential equation.

$$\frac{\partial \vec{M}_i}{\partial t} \quad \gamma_i \bullet \vec{M}_i \times H_{effi} + \frac{\left(\alpha_{Gi} + \alpha_{spi}\right)}{M_{si}} \bullet \vec{M}_i \times \frac{\partial \vec{M}_i}{\partial t} \tag{22}$$

exactly describes the motion of the magnetic moments which are inhibited in precession by the damping parameters α_G and α_{spi}. Solving the LLG a measure of precession can be deduced in the form of the real– and imaginary part of the frequency-dependent permeability. The maximum of the imaginary part represents the ferromagnetic resonance frequency.

$$f_{FMRi} \quad \frac{\gamma_i}{2\pi \bullet \left(1 + \left(\alpha_{Gi} + \alpha_{spi}\right)^2\right)} \bullet \mu_0 \bullet H_{effi}$$

$$\frac{\gamma_i}{2\pi \bullet \left(1 + \left(\alpha_{Gi} + \alpha_{spi}\right)^2\right)} \bullet \mu_0 \bullet \sqrt{H_{ui}^2 + H_{ui} \bullet M_{si} \quad \left(\alpha_{Gi} + \alpha_{spi}\right)\frac{M_{si}^2}{4}} \tag{23}$$

of the ith ferromagnetic layer. For the Gilbert (bulk) and spin current damping parameters, we can use the following expressions according to [16].

$$\alpha_{Gi} \quad \frac{2\pi}{\gamma_i} \bullet \frac{\Delta f_{sri}}{(J_{si} + \mu_0 \bullet H_{ui})} \tag{24}$$

and.

$$\alpha_{spi} \quad \frac{2\pi}{\gamma_i \bullet (J_{si} + \mu_0 \bullet H_{ui})} \bullet (\Delta f_{FMRi} \quad \Delta f_{sri}) \tag{25}$$

whereas Δf_{sri} is the full width at half maximum of the ith imaginary part of the film deposited as a single layer and Δf_{FMRi} the full width at half maximum (FWHM) of the ith film at ferromagnetic resonance in the film stack, respectively. Both FWHMs are quantifiable from the measured frequency spectra. If the exchange interaction between the film layers are weak, two individual resonances are expected.

In order to plot the effective damping parameter of the ferromagnetic layer "i" on the dependence of the interface layer thickness, the following general expression can be applied.

$$\alpha_{eff}^i \quad \alpha_{Gi} + \alpha_{spi} \text{ i } \quad 1,2 \text{ (26)}.$$

Analogously to [6,17], we establish the definition.

$$\alpha_{eff}^i \quad \alpha_{Gi} + \alpha_{sp}^i \bullet \left(\frac{S_{xy}^{ref/trans}}{S_{xy}^{ref/trans}(t_{int} \quad 0)}\right) \tag{27}$$

which leads to the phenomenological behaviour of the effective damping parameter of each ferromagnetic layer. The term in brackets describes the normalised reflection/transmission of spins currents through the tunnel barrier, which may contribute to damping enhancement or anti-damping of the precessing magnetic moments of each ferromagnetic layer, respectively.

3. Experimental set of tools

Soft ferromagnetic trilayer $Ni_{80}Fe_{20}/Si_3N_4/Fe_{40}Co_{37}Zr_{11}N_{12}$ film systems were deposited on Si (1 0 0) substrates with 1 μm silicon oxide (5 mm × 5 mm × 0.375 mm) by reactive r.f. magnetron sputtering in an Ar/N_2 atmosphere at a constant pressure of 0.5 Pa. The sputtering power was 250 W and the argon/nitrogen gas flow fraction was kept constant at about 70 sccm/1sccm. For $Ni_{80}Fe_{20}$ only Ar served as a sputtering gas by using the same pressure and power. For deposition, 6-inch targets (target composition in at.-%: $Fe_{37}Co_{46}Zr_{17}$, $Ni_{80}Fe_{20}$) were used in a Leybold Heraeus Z550 sputtering device. In order to deposit the nonmagnetic interface layer system Si_3N_4, a 6-inch target was utilised. The film thickness was determined by means of a TENCOR P-10 Surface Profiler. Thereby, a sputtering rate could be detected which enabled the estimation of the particular layer thickness.

An annealing process at 400 °C for 2 h in a static magnetic field (~50 mT) was carried out, in order to generate an in-plane uniaxial anisotropy in the film plane by arranging a short-range order of Fe and Co transition elements, respectively [18]. The polarisation loops J($\mu_0 H_{ext}$) $\mu_0 M$ (M is the magnetisation) of the easy and hard direction of the magnetic polarisation were measured by means of a Quantum Design VersaLab vibrating sample magnetometer (VSM). The high-frequency permeability was measured with a strip-line permeameter designed for frequencies up to 5 GHz [19,20]. It is connected to one port of an Agilent 8753 ES network analyser.

4. Experimental results and discussion

4.1. The static magnetisation

In contrary to the single film layers $Ni_{80}Fe_{20}$, $Fe_{40}Co_{37}Zr_{11}N_{12}$ or $Ni_{80}Fe_{20}/Fe_{40}Co_{37}Zr_{11}N_{12}$ bilayers [16], the polarisation behaviour of a trilayer configuration appears differently. The saturation polarisation J_s $\mu_0 M_s$ of $Ni_{80}Fe_{20}/Si_3N_4/Fe_{40}Co_{37}Zr_{11}N_{12}$ results in around 1.3 T. This is between J_s 1 T for $Ni_{80}Fe_{20}$ and J_s 1.5 T for $Fe_{40}Co_{37}Zr_{11}N_{12}$. Regarding the hard axis of polarisation, the in-plane uniaxial anisotropy of the two ferromagnetic layers are implied by two inflection points. The uniaxial anisotropy fields $\mu_0 H_u$ are around 0.5 mT ($Ni_{80}Fe_{20}$) and 4.0 mT ($Fe_{40}Co_{37}Zr_{11}N_{12}$). The separation with an insulating Si_3N_4 interface layer causes two slopes in the hard direction of polarisation (Fig. 3 a-c). The slopes become tighter if the exchange interaction energy between the magnetic layers diminishes with an increased interlayer thickness.

The theoretical calculations J($\mu_0 H_{ext}$) $\mu_0 M$ of the hard axis polarisation qualitatively demonstrate that they are in a good agreement with the experimental data. The detailed and aggregate expressions for the numerically computed polarisation fit can be found in [16]. Beside the measured saturation polarisation values of the single ferromagnetic films listed above the uniaxial anisotropy coefficients $K_u \approx 75$ J/m^3 for $Ni_{80}Fe_{20}$ and $K_u \approx 1900$ J/m^3 for $Fe_{40}Co_{37}Zr_{11}N_{12}$ are used as additional fit parameters. The exchange energy parameter between the ferromagnetic layers drops within the 10^{-5} J/m^2 range, and the lower the exchange the more angular the hard axis loop, i.e., the magnetisation vectors of the layers rotate independently. By considering the easy axis of polarisation, although, it exhibits a soft magnetic behaviour two kinks appear which are more distinctive if the Si_3N_4 interface layer is thicker. Obviously, the magnetic moments switch in two steps, which causes pinning of magnetic moments by increasing interface roughness. Roughness also generates a microscopic demagnetisation process, which originates from the "orange-peel" effect. One can observe that the magnetisation becomes slightly harder due to perturbation by the rippled interface, which impacts the magnetic order. Although, this effect can slightly alter the easy axis of magnetisation, it does not appreciably generate dipolar coupling, which can be estimated by [21] and which is in the range of 10^{-10} J/m^2 to 10^{-20} J/m^2. Consequently, one can neglect the dipolar energy.
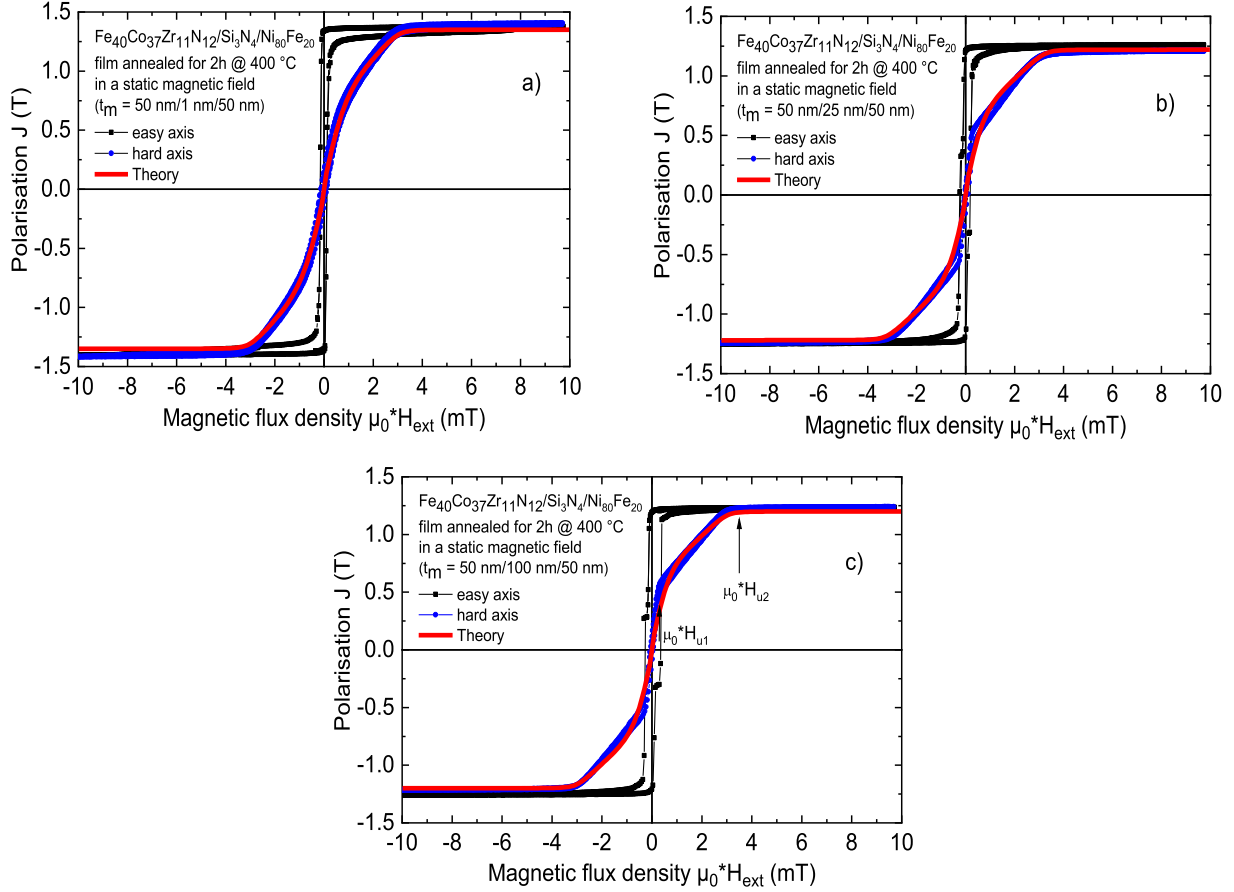
Fig. 3. Hard and easy axis polarisation loops of $Ni_{80}Fe_{20}/Si_3N_4/Fe_{40}Co_{37}Zr_{11}N_{12}$ trilayer films, which were annealed at 400 °C for 2 h in an external static magnetic field. The in-plane uniaxial anisotropy field is approximately indicated by arrows, e.g. in c). The individual layers possess a thickness of a) 50 nm/1 nm/50 nm, b) 50 nm/25 nm/50 nm and c) 50 nm/100 nm/50 nm, respectively. The thick solid lines show the theoretical polarisation behaviour of the hard axis [16].

4.2. The dynamic magnetisation

In the following section, the investigation is concentrated on the high-frequency spectra. Two resonance peaks appear at around 0.6 GHz and 2.3 GHz, respectively. These resonance frequencies are close to single film resonance frequencies observed in [16] for which their Gilbert damping parameters α_G are 0.017 for $Ni_{80}Fe_{20}$ and 0.0062 for $Fe_{40}Co_{37}Zr_{11}N_{12}$. In Fig. 4 a) to c), two resonance peaks can be identified which represent the individual dynamic feature of the ferromagnetic layers in the film stack due to the uniaxial anisotropies and weak ferromagnetic layer exchange interaction between the magnetic layers. Increasing the interface layer thickness the resonance peaks are more and more defined which reflects the decreasing exchange energy. It is noteworthy that even the shapes of the resonance peak visibly change if the interface layer gets thicker. As clearly observed, the FWHM of the $Ni_{80}Fe_{20}$ peak is lower than the FWHM of the $Fe_{40}Co_{37}Zr_{11}N_{12}$ resonance peak. The maximum of the two peaks nearly equalises if the interface layer becomes thicker and the FWHM values hereupon shape up in the opposite direction. By virtue of this conspicuous phenomenon, one can assume that mutual spin currents cause high-frequency precession damping and anti-damping in the individual ferromagnetic layers. Fig. 5 shows that the magnetic moments of $Ni_{80}Fe_{20}$ generate lower FWHM for less Si_3N_4 interface layer thickness than being in the single layer configuration, which exponentially increases if Si_3N_4 becomes thicker. For $Fe_{40}Co_{37}Zr_{11}N_{12}$, the FWHM exponentially decreases and saturates at around the same Si_3N_4 layer thickness. In Fig. 5, one can also find the FWHM levels of the single layer systems for comparison, indicated by the dashed lines. If $Ni_{80}Fe_{20}$ is on resonance a lower FWHM than Δf_{FMR} of the single layer, which accounts to 0.356 GHz, was observed up to

approximately t_{int} 10 nm interface layer thickness. The FWHM Δf_{FMR} now exceeds 0.356 GHz and saturates at around 40 nm. On the other hand, $Fe_{40}Co_{37}Zr_{11}N_{12}$ appears in enhanced FWHM for the interface layer thickness up to around t_{int} 10 nm. At higher thickness, the FWHM declines below the nominal single film Δf_{FMR} of 0.341 GHz and comparably saturates at 40 nm.

This behaviour reflects the effective damping parameters α_{eff}, which delivers the direct indication of damping and anti-damping due to a spin current flow. Although, a possible spin current between the ferromagnetic layers in the present tunnel system decays exponentially within a few nanometres, for all that its impact on the damping behaviour cannot be rationalised away.

By means of the data in Fig. 5 and according to expressions (25) and (26) the individual effective damping parameters could be determined and then plotted in Fig. 6.

According to the behaviour of tunnelling and by taking (27) into account for the data fit it is observable that the theoretical estimation is in a good agreement with the determined effective damping parameters. Regarding the effective damping parameter data, they strongly increase or decline within this range. For the fit calculations, we assumed a Fermi energy EF of about $1.538 \cdot 10^{-18}$ J for $Ni_{80}Fe_{20}$ [22] and approximately a mean EF $1.535 \cdot 10^{-18}$ J for the Fe-Co phase [23,24]. The potential barrier height Ub generated by the Si_3N_4 interface layer is determined to be $1.545 \cdot 10^{-18}$ J according to Fig. 1 by employing a Fermi energy of $1.121 \cdot 10^{-18}$ J and an energy gap E_g of $8.49 \cdot 10^{-19}$ J [25,26]. So, the energy of the tunnelling spins are very close to the barrier height which imparts the vicinity to resonant tunnelling indicated in Fig. 2. To all appearance, the effective damping parameter allusively reflects this behaviour as one cannot observe a steady increase or decrease of the damping data on the
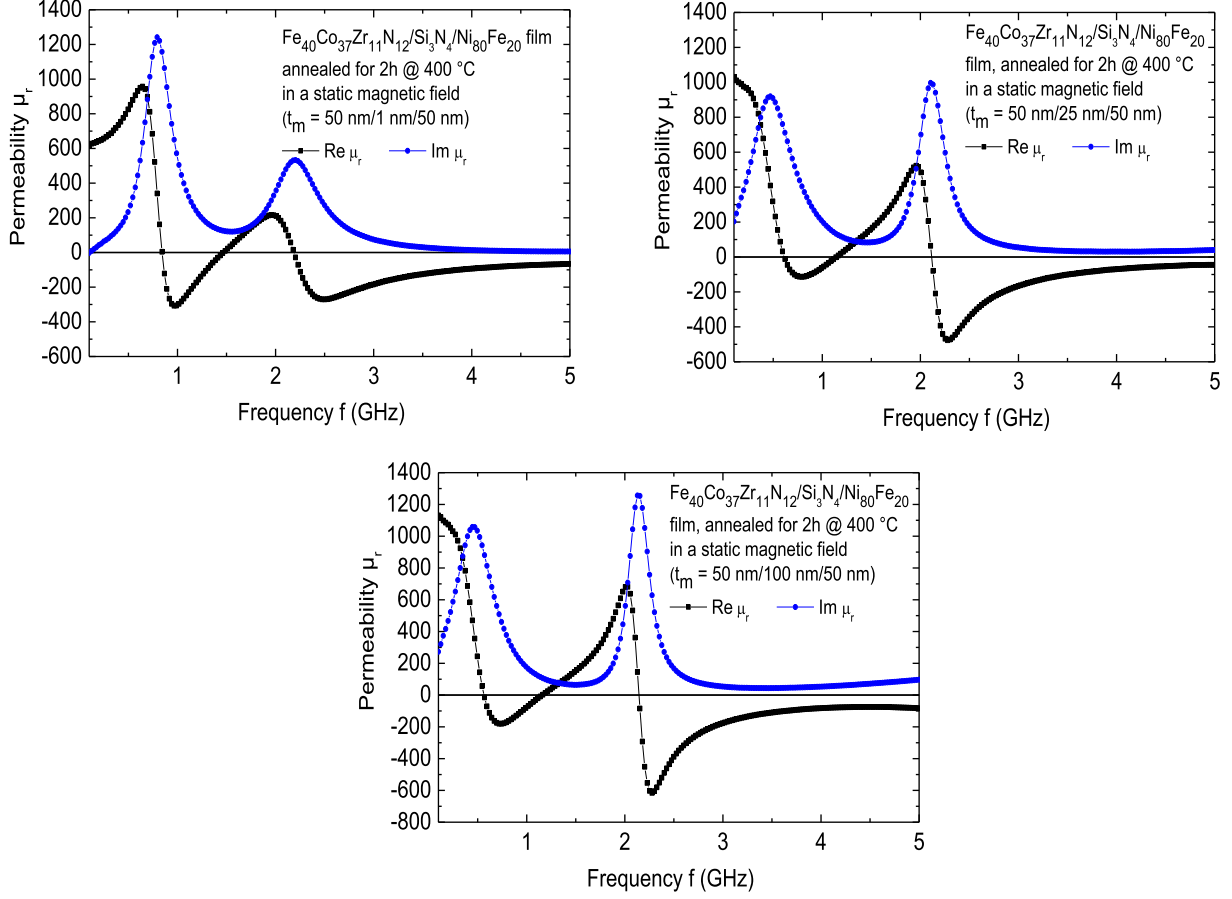
Fig. 4. Real- and imaginary part of the frequency-dependent permeability of $Ni_{80}Fe_{20}/$ $Si_3N_4/Fe_{40}Co_{37}Zr_{11}N_{12}$ trilayer films. The individual layers possess a thickness of a) 50 nm/1 nm/50 nm, b) 50 nm/25 nm/50 nm and c) 50 nm/100 nm/50 nm, respectively.
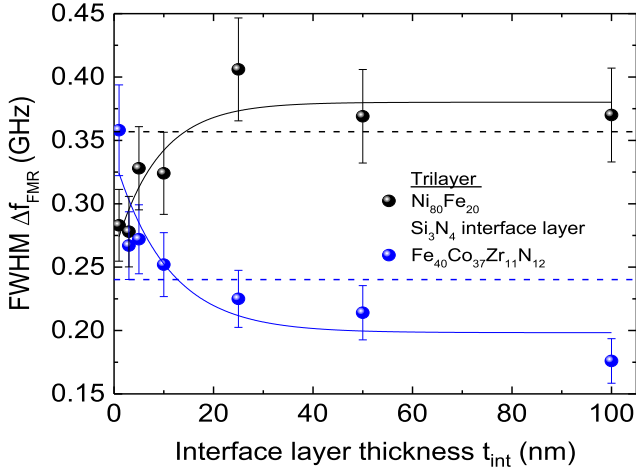

Fig. 5. Full width at halve maximum of the imaginary part of the frequency-dependent permeability of $Ni_{80}Fe_{20}/Si_3N_4/Fe_{40}Co_{37}Zr_{11}N_{12}$ trilayer layer films dependent on the Si_3N_4 interface layer thickness. The dashed horizontal lines indicate the FWHM of the single films. The error bars show an uncertainty of 10 %.

dependence of the interface layer thickness which comes from the slight maxima and minima (see enlargement Fig. 6). If $Ni_{80}Fe_{20}$ is on resonance, the spin current flows through the barrier with thickness below 10 nm and faces a bad $Fe_{40}Co_{37}Zr_{11}N_{12}$ spin sink. It causes backflow resulting in a negative spin current damping parameter. Here, we assumed that reflection of spins across the barrier is effective. Based on the damping behaviour of the bilayer with t_{int} 0 [16], we estimated $\alpha_{sp}(t_{int}$ 0) -0.006 for $Ni_{80}Fe_{20}$. By increasing the barrier thickness, the spin current damping parameter approaches zero while the spins lose more and more angular momentum and α_{eff} converges the Gilbert damping parameter α_G 0.017. If the $Fe_{40}Co_{37}Zr_{11}N_{12}$ layer is on resonance, $Ni_{80}Fe_{20}$ seems to be a good spin sink for spins tunnelling through a thin barrier < 5 nm, until the Gilbert damping parameter reaches the single film value of around 0.0062 at a higher barrier thickness. Here, the transition of spins is responsible for the increased effective damping parameter. Consequently, spin current initially generates enhanced damping $\alpha_{sp}(t_{int}$ 0) of about 0.0048, and it swiftly vanishes with an increased barrier thickness. Looking at the rise or drop of α_{eff} it can be assumed that a decay length λ_d of the electron spins in the interface layer Si_3N_4 must be clearly below 5 nm.

From around t_{int} 50 nm, it cannot be ignored that α_{eff} continually drops which obviously can be attributed to backscattering into the $Fe_{40}Co_{37}Zr_{11}N_{12}$ on-resonance layer. Hence, α_{sp} seems to become negative as well, as it falls below the nominal Gilbert damping value.

5. Conclusion

In order to obtain a good high-frequency suitability of soft ferromagnetic films, they have to feature a defined in-plane uniaxial anisotropy. This moves the ferromagnetic moments as being uniformly magnetised by an external magnetic field. In general, the films are magnetically saturated. Additionally, they exhibit a soft magnetic behaviour and consequently, it results in sharp frequency dependent permeability spectra.

A maximum spin current flow between two ferromagnetic film layers is generated if at least one layer is on ferromagnetic resonance. If an
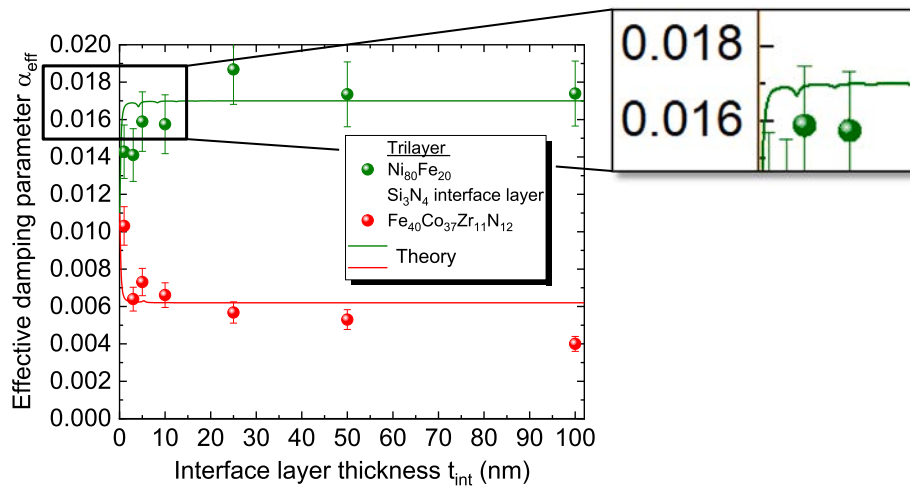
Fig. 6. Damping parameter α_{eff} of the $Ni_{80}Fe_{20}/Si_3N_4/Fe_{40}Co_{37}Zr_{11}N_{12}$ trilayers dependent on the interface layer thickness, t_{int}. The solid curves show the theoretical calculations for α_{eff}. The error bars show an uncertainty of 10 %.

insulating interface layer, acting as a tunnelling barrier, separates the ferromagnetic layers the spin current can tunnel between the layers. An approach was made by a tunnelling model in combination with a potential step, which shows a swift decay of the spin current density. High-frequency permeability measurements reflect that a spin current mutually influences the FWHM of the resonance peaks. The efficient precession damping parameter shows an enhancement of effective damping for $Ni_{80}Fe_{20}$ and a reduction for $Fe_{40}Co_{37}Zr_{11}N_{12}$ within 5 nm. This is in a good qualitative agreement with the model. As a result, the additional spin pumping damping parameter α_{spi} for $Ni_{80}Fe_{20}$ is negative by backflow of spins while for $Fe_{40}Co_{37}Zr_{11}N_{12}$ it has a positive sign. This means, that $Ni_{80}Fe_{20}$ acts as a spin sink or "spin brake" which increases α_{eff} for $Fe_{40}Co_{37}Zr_{11}N_{12}$ until it reaches it nominal value of the single layer at a higher interface layer thickness.

Then again, $Fe_{40}Co_{37}Zr_{11}N_{12}$ does not seem to be a good spin sink. Nevertheless, it is remarkable that its effective damping parameter falls short of the nominal single layer value due to a presumable sudden spin current backflow.

CRediT authorship contribution statement

K. Seemann: Conceptualization, Data curation, Formal analysis, Funding acquisition, Investigation, Methodology, Project administration, Resources, Software, Supervision, Validation, Visualization, Writing – original draft, Writing – review & editing.

Declaration of Competing Interest

The authors declare that they have no known competing financial interests or personal relationships that could have appeared to influence the work reported in this paper.

Data availability

No data was used for the research described in the article.

References

[1] C. Bechtold, I. Teliban, C. Thede, S. Chemnitz, E. Quandt, Sens. Actuators A 158 (2010) 224.
[2] S. Beirle, K. Seemann, Sens. Actuators A 301 (2020), 111788.
[3] A. Garcia-Arribas, L. Combarro, M. Goiriena,-Goikoetxea, G. V. Kurlyandskaya,A. V. Svalvo, E. Fernández, I. Orue, J. Feuchtwanger, 2017 *IEEE Trans. Magn.* **53** 2000605.
[4] B. Heinrich, Y. Tserkovnyak, G. Woltersdorf, A. Brataas, R. Urban, G.E.W. Bauer, Phys. Rev. Lett. 90 (2003) 187601–187611.
[5] Y. Tserkovnyak, A. Brataas, G.E.W. Bauer, B.I. Halperin, Rev. Mod. Phys. 77 (2005) 1375.
[6] J. Foros, G. Woltersdorf, B. Heinrich, A. Brataas, J. Appl. Phys. 97 (2005) 10A714–11.
[7] H. Nakayama, K. Ando, K. Harii, T. Yoshino, R. Takahashi, Y. Kajiwara, K. Uchida, Y. Fujikawa, E. Saitoh, Phys. Rev. B 85 (2012), 144408.
[8] C. Swindells, A.T. Hindmarch, A.J. Gallant, D. Atkinson, Phys. Rev. B 99 (2019), 064406.
[9] C.H. Du, H.L. Wang, Y. Pu, T.L. Meyer, P.M. Woodward, F.Y. Yang, P.C. Hammel, Phys. Rev. Lett. 111 (2013), 247202.
[10] A.A. Baker, A.I. Figueroa, L.J. Collins-McIntyre, G. van der Laan, T. Hesjedal, Sci. Rep. 5 (2015) 7907.
[11] A.I. Figueroa, A.A. Baker, L.J. Collins-McIntyre, T. Hesjedal, G. van der Laan, J. Magn. Magn. Mater. 400 (2016) 178.
[12] A.A. Baker, A.I. Figueroa, D. Pingstone, V. K. Lazarov, G. van der Laan, T, Hesjedal, 2016 *Sci. Rep.* **6** 35582.
[13] C. Swindells, A.T. Hindmarch, A.J. Gallant, D. Atkinson, Appl. Phys. Lett. 116 (2020), 042403.
[14] M.D. Stiles, A. Zangwill, Phys. Rev. B 66 (2002) 014407–014411.
[15] D.C. Ralph, M.D. Stiles, J. Magn. Magn. Mater. 320 (2008) 1190.
[16] K. Seemann, J. Magn. Magn. Mater. 529 (2021), 167850.
[17] A. Kumar, S. Akansel, H. Stopfel, M. Fazlali, J. Akerman, R. Brucas, P. Svedlindh, Phys. Rev. B 95 (2017) 064406–064411.
[18] K. Seemann, S. Beirle, H. Leiste, J. Magn. Magn. Mater. 413 (2016) 115.
[19] V. Bekker, K. Seemann, H. Leiste, J. Magn. Magn. Mater. 270 (2004) 327.
[20] Y. Liu, L. Chen, C.Y. Tan, H.J. Liu, C.K. Ong, Rev. Sci. Inst. 76 (2005), 063911.
[21] J.C.S. Kools, W. Kula, J. Appl. Phys. 85 (1999) 4466.
[22] G.V. Paradezhenko, D. Yudin, A.A. Pervisko, Phys. Rev. B 104 (2021), 245102.
[23] K. Schwarz, P. Mohn, P. Baha, J. Kübler, J. Phys. F: Met. Phys. 14 (1984) 2659.
[24] S.E. Kulkovaa, D.V. Valujskya, J.S. Kimb, G. Leeb, Y.M. Koob, Physica B 322 (2002) 236.
[25] S. Miyazaki, M. Narasaki, A. Suyama, M. Yamaoka, H. Murakami, Appl. Surf. Sci. 216 (2003) 252.
[26] B. Roul, M. Kumar, M. Rajpalke, T. Bhat, S. Krupanidhi, J. Phys. D: Appl. Phys. 48 (2015), 423001.